ANL/ASD/CP--90188
CONF-9605173--18

Commissioning Results of the APS Storage Ring Diagnostics Systems*

RECEIVED
FEB 20 1997
OSTI

A. H. Lumpkin

Advanced Photon Source, Argonne National Laboratory
9700 South Cass Avenue, Argonne, Illinois 60439 USA

Abstract. Initial commissionings of the Advanced Photon Source (APS) 7-GeV storage ring and its diagnostics systems have been done. Early studies involved single-bunch measurements for beam transverse size ($\sigma_x \approx 150$ μm, $\sigma_y \approx 50$ μm), current, injection losses, and bunch length. The diagnostics have been used in studies related to the detection of an extra contribution to beam jitter at ~ 6.5 Hz frequency; observation of bunch lengthening ($\sigma \approx 30$ to 60 ps) with single-bunch current; observation of an induced vertical, head-tail instability; and detection of a small orbit change with insertion device gap position. More recently, operations at 100-mA stored-beam current, the baseline design goal, have been achieved with the support of beam characterizations.

MASTER

INTRODUCTION

The commissioning of the Advanced Photon Source (APS) 7-GeV storage ring (SR) was supported by a full complement of diagnostics subsystems (1-3). Both the machine and, in some cases, specific features of the diagnostics systems were evaluated and demonstrated in a phased manner. Essential steps of first injected beam, first single turns, first multiple turns, stored beam, and increased stored beam were tracked with generally standard measurement techniques. However, assistance from the single-turn rf beam position monitor (BPM) capability and the functioning photon monitor for optical synchrotron radiation (OSR) imaging for transverse beam size measurements and early bunch length measurements were very useful, particularly in the single-bunch, first-turn measurements. Early studies included single-bunch measurements for beam transverse size, orbit stability, current, injection losses, and bunch length. The detection and resolution of an unexpected horizontal beam motion contribution at ~ 6.5 Hz frequency as revealed through analysis of rf BPM data (4) is addressed as well as bunch lengthening effects with single-bunch current and an induced vertical, head-tail instability. The path traveled to get both the machine and the diagnostics functioning at the baseline, 100-mA stored-beam current is also discussed.

* Work supported by U. S. Department of Energy, Office of Basic Energy Sciences under Contract No. W-31-109-ENG-38.

DISTRIBUTION OF THIS DOCUMENT IS UNLIMITED

The submitted manuscript has been authored by a contractor of the U. S. Government under contract No. W-31-109-ENG-38. Accordingly, the U. S. Government retains a nonexclusive, royalty-free license to publish or reproduce the published form of this contribution, or allow others to do so, for U. S. Government purposes.

DISCLAIMER

Portions of this document may be illegible in electronic image products. Images are produced from the best available original document.

EXPERIMENTAL BACKGROUND AND PROCEDURES

The APS storage ring diagnostics include a full complement of subsystems. As shown in Fig. 1, there are 360 rf BPMs, one direct-current current transformer (DCCT), ten intercepting profiling screens with cameras, two striplines for tune measurements, five scrapers, ten loss rate monitors, and an installed OSR imaging station on a bending magnet source. As a comment in passing, a subset of this figure was shown in the 1992 BIW (2), but at that point they were only planned; now all are installed and functional except the undulator radiation source and beamline. Basic accelerator parameters for diagnostics are listed in Table 1. The fundamental rf frequency is 351.9 MHz with a harmonic number of 1296 in the 1104-m-circumference ring. The horizontal and vertical damping times are 9.4 ms with horizontal and vertical tunes being 35.22 and about 14.30, respectively. The longitudinal damping time is 4.7 ms at 7 GeV and the synchrotron frequency is about 1.9 kHz, depending on the rf gap voltage. The baseline design was for 5 mA (18 nC) in a single bunch with 20 bunches to make the 100-mA design goal. However, we typically find better lifetimes with a fill of at least 36 bunches and often use a few hundred. There are 40 sectors in the ring with the injection point in sector 40 and the first insertion device in sector 1.

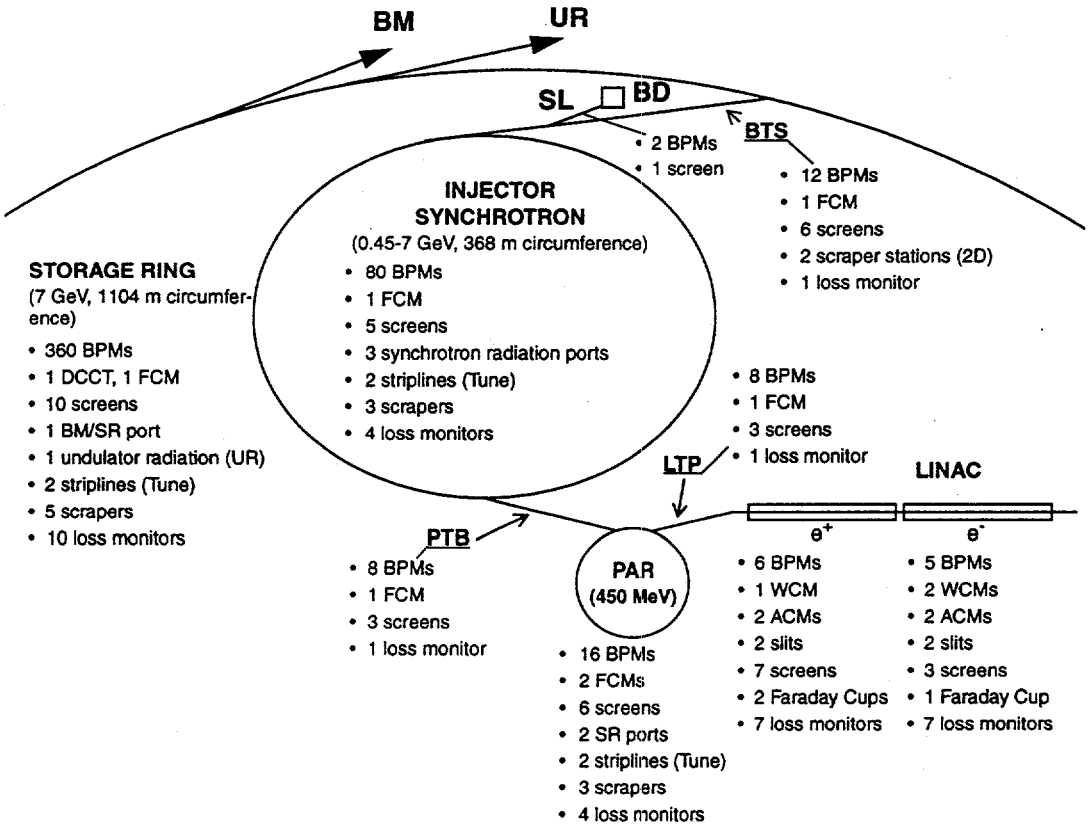

FIGURE 1. Schematic of beam diagnostics in the APS.

TABLE 1. Accelerator Parameters for Diagnostics

Parameter	Storage Ring	Inj. Synch.
Energy (GeV)	7	0.45 - 7
RF Freq. (MHz)	351.93	351.93
Harmonic No.	1296	432
Min. Bunch Spacing (ns)	2.8	1228
Rev. Period (μs)	3.68	1.228
No. of Bunches	1-1296	1
Design Max. Single Bunch Current (mA)	5	4.7
Bunch Length (2σ) (ps)	35-100	61-122
Damping Times $\tau_{h,v}$ (ms)	9.46	2.7 @ 7 GeV
Tunes υ_h, υ_v	35.22, 14.30	11.76, 9.80
Damping Time τ_s (ms)	4.73	1.35 @ 7 GeV
Synch. Freq. f_s (kHz)	1.96	21.2

Beam Profile Monitors

Beam profile monitors are based on intercepting, chromox screens viewed by standard Vicon charge-coupled device (CCD) cameras. For initial injection, camera stations in sectors 40, 1, 7, 14, and 39 supported transport through the first third of the ring and then the S39 flag supported evidence for the first full turn. (In fact, the OSR port in sector 35 was used to monitor the first turn.)

Beam Position Monitors

Beam position monitors are located in all 40 sectors around the ring. There are 360 stations using rf BPM button pickups and their associated electronics. The storage ring standard vacuum chamber uses 10-mm-diameter button feedthroughs, and the insertion device vacuum chambers (IDVC) use 4-mm-diameter buttons. The BPM electronics have been designed for single-turn capability using a monopulse receiver that involves the amplitude to phase conversion technique. In stored beam mode, a separate module with a boxcar averager can process values from the nine signal conditioning and digitizing units (SCDUs) in each VXI crate for each sector. Very good position resolution has been achieved which will be briefly discussed in the next section and more completely in reference (5).

Beam Current Monitors

Monitoring of the current/charge in the transport lines and injector rings is generally based on the use of fast current transformers (FCTs) manufactured by Bergoz, shielded housings, and in-house electronics (6). In the storage ring a Bergoz parametric current transformer (PCT) Model PCT-S-175 is the basis of the DC current measurement. Additionally, an integrating current transformer (ICT) is mounted in the same housing as the DCCT and allows single-bunch evaluation of charge in the SR.

Beam Loss Rate Monitors

The beam loss rate monitors (LRMs) cover the transport line from the booster to storage ring (BTS) as well as the circumference of the ring in 10 sections. A gas-filled coaxial cable acting as an ionization chamber is used to detect bremsstrahlung radiation. In practice, it is also sensitive to the hard storage ring x-rays; so for stored beam conditions, specific losses are more difficult to identify. This system is discussed in more detail elsewhere in these proceedings (7).

Synchrotron Radiation Monitors

Transverse beam profiles and bunch lengths have been measured using OSR and x-ray synchrotron radiation (XSR) imaging techniques. A bending magnet source is dedicated to particle beam characterization. The early commissioning data were taken using an OSR pick-off mirror based on a water-cooled Moly assembly. A standard Vicon CCD camera linked to a Questar telemicroscope was initially used within the accelerator tunnel (8). Subsequently, an in-air transport line with a series of mirrors was used to bring the OSR out of the tunnel and onto an optical diagnostics table for measuring with a CCD camera and the Hamamatsu C5680 dual-sweep streak camera.

The main features of the dual-sweep streak system include a synchroscan sweep unit phase-locked to the 117.3-MHz source from the rf system oscillator. On its fastest range it has a resolution $\sigma_{res} \sim 0.6$ ps with time jitter expected to be less than that. The four selectable ranges have a time axis span of 0.15 to 1.5 ns. The slow sweep axis can be triggered at up to 10 Hz with a selection of time spans from 100 ns to 100 ms. For single-bunch experiments with a ring circulation time of 3.68 μs, the 10-, 20- and 100-μs ranges were often used. The streak images were read-out at the standard 30-Hz video rate using a Peltier-cooled CCD chip camera. Controls were done through a GPIB interface to the local computer. The

video images were also shipped via the video mux to the main control room for on-line display on TV monitors.

By the time of the high current runs, a second split mirror was installed for the OSR pick-off to the streak camera, and an x-ray pinhole imaging station was operational within the tunnel as described in an accompanying paper in these proceedings (9).

PRIMARY DIAGNOSTICS AND INITIAL COMMISSIONING OF THE STORAGE RING

As mentioned earlier, the primary diagnostics were used for initial injection and first turns. The DCCT, five intercepting screens, the loss rate monitors, over 300 rf BPMs with single-turn capability, and a single-turn OSR monitor were available. Early in machine commissioning we also addressed key issues of rf BPM resolution, beam stability, transverse size, and bunch length which will be discussed in more detail below.

rf BPM Resolution Tests

In stored-beam mode the resolution of the rf BPM monitors can be effectively improved by averaging over many turns or increasing the beam charge in the ~ 50-ns-wide integration window of the electronics. The details of the electronics are covered elsewhere and a more complete report is given in these proceedings (5). The assessment of contributions from electronics noise versus actual beam motion was facilitated by deliberately cross-connecting selected cables to the front-end rf BPM buttons at a location. By crossing the top two buttons in S6B:P1, rotating by 90° the connections in S6A:P1, and crossing the inboard buttons in positions S9A:P1 and S9B:P1, the 4-button set's sensitivity to beam motion in the horizontal plane is nulled, the vertical goes to horizontal in the electronics, and the vertical plane is nulled, respectively. The sector 7 rf BPMs had all normal connections. The BPM resolution was then evaluated at fixed current and N turns or with fixed average and varied beam current. Examples of the results are shown in Fig. 2. In Fig. 2(a) the reduction of the variance in the averages of measurements Δx, Δy are shown versus sampling number N. An approximate $1/\sqrt{N}$ slope is seen down to ~ 8 μm at 2048-turn average for the S6B:P1:x data and the S9B:P1:y data with their insensitivities to x and y motion, respectively. The sector 7 x data do not follow this but flatten out at about 30 μm. This was attributed to actual horizontal beam motion of about 30 μm rms. In Fig. 2(b), the averaging at N = 2 turns is fixed and the approximate inverse dependence on beam current (I_b) is exhibited. Again the sector 7 x and y data do not follow the trend like the S6B:P1:x and the

S9B:P1:y data. Actual beam motion in the two planes adds to the variance in the x position. This 30-μm rms horizontal motion was actually beyond the orbit stability specification and will be addressed in the next section. The summary results of the rf BPM resolution is that the electronic contribution to resolution is about

$$\Delta x_e \sim \left\{ \begin{array}{ll} 0.16 & \text{regular} \\ 0.1 & \text{ID} \end{array} \left[\frac{\mu m \cdot mA}{\sqrt{Hz}} \right] \right\} \times \frac{\sqrt{BW}}{I_b[mA]}. \tag{1}$$

That is, for regular rf BPM buttons in a normal gap vacuum chamber for 2-mA beam and 100-Hz bandwidth (BW), a resolution of 0.8 μm is expected. It is 60% lower for the miniature rf BPM locations. This result can be compared to the baseline orbit stability specification of 17 μm horizontally and 4 μm vertically (rms). Additional issues of offset long-term drift, bunch pattern dependency, and beam intensity dependence are being evaluated (5).

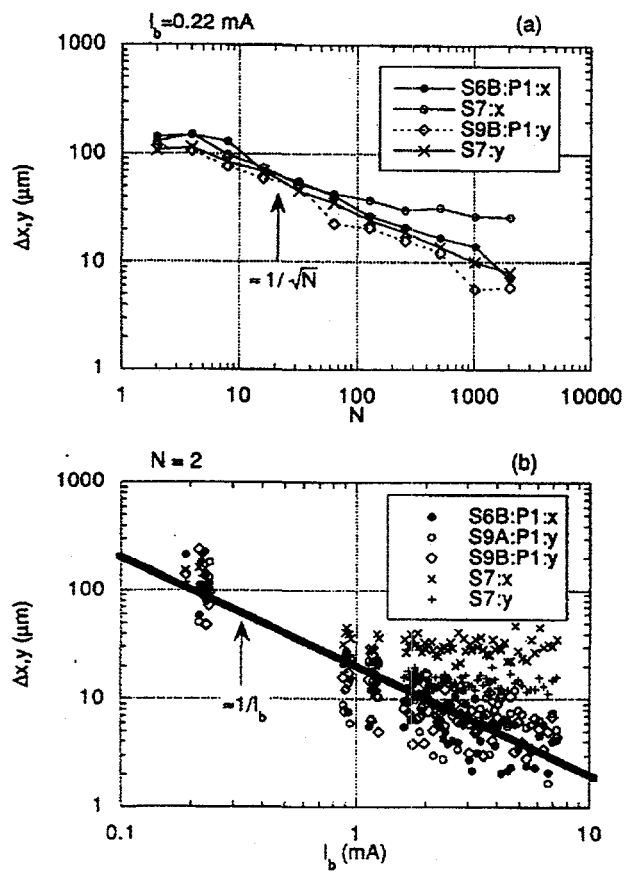

FIGURE 2. Results of rf BPM resolution tests for (a) fixed current and various averages of multiple turns and (b) fixed average and varying current.

Beam Stability

As noted in the previous section, evidence for rms-horizontal beam motion of about 30 μm was detectable in these resolution tests. It had been detected earlier in commissioning by examining the frequencies of beam motion contributions using a vector signal analyzer (1). The rf BPM system is able to detect rms beam motion with resolution better than 4 μm in the 1-20 Hz band. Figure 3 shows the frequency analysis of this motion by plotting the power log10(V) versus delta frequency with 135.7 kHz the center (carrier) frequency. Noticeable broad peaks at ± 6.5 Hz are seen as well as at about 11 Hz, the girder vibration contribution. A search for the source including the BPM electronics was undertaken. By sampling the performance of the various classes of power supplies for the magnet sets in the ring, it was noticed that the sextupoles (family 1) had a strong correlation to the problem. Figure 4 shows the decrease in the observed beam motion by turning off the power supplies. In fact, with them off the rms motion was below 20 μm. A representative sextupole power supply's noise was analyzed for frequency content, and a spike at 6.5 Hz was found. The sextupole regulators were modified with an additional filter, and in October of 1995 the upgrades were completed. Figure 5 shows an example of the motion frequency contents before and after the upgrade. As shown in Table 2, the rms motion in the 1→15 Hz band dropped from 27 to 15.5 μm. This rather unanticipated effect was related to current ripple of the S1A sextupoles at 5→8 Hz.

The eddy current induced by the ripple field in the sextupole produced a vertical dipole field to drive the beam horizontally. It is noted the extruded vacuum chamber is horizontally nonsymmetric (4).

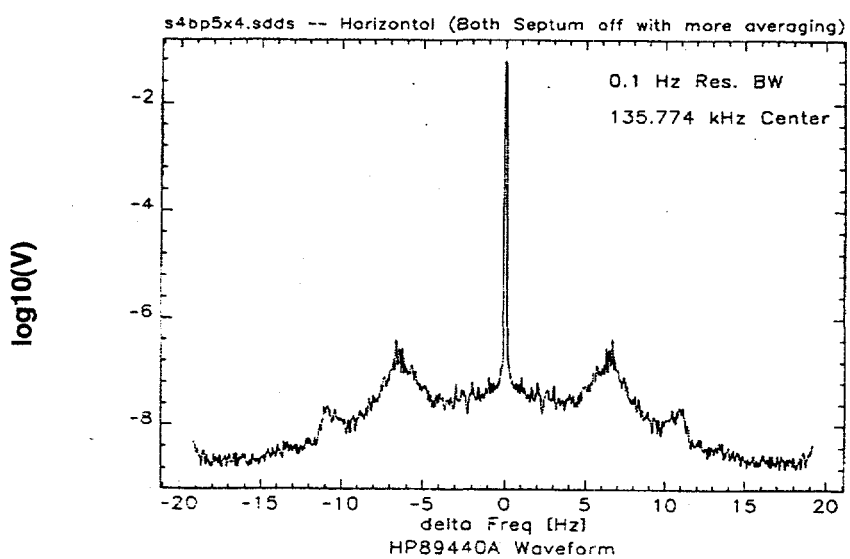

FIGURE 3. Frequency analysis of observed beam motion using the vector signal analyzer processing the rf BPM signals.

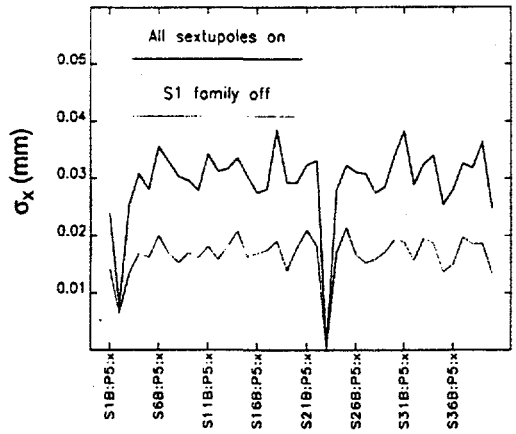

FIGURE 4. Comparison of rms beam motion with sextupole family S1 on and off. The lighter curve (S1 off) shows motion below 20 μm rms.

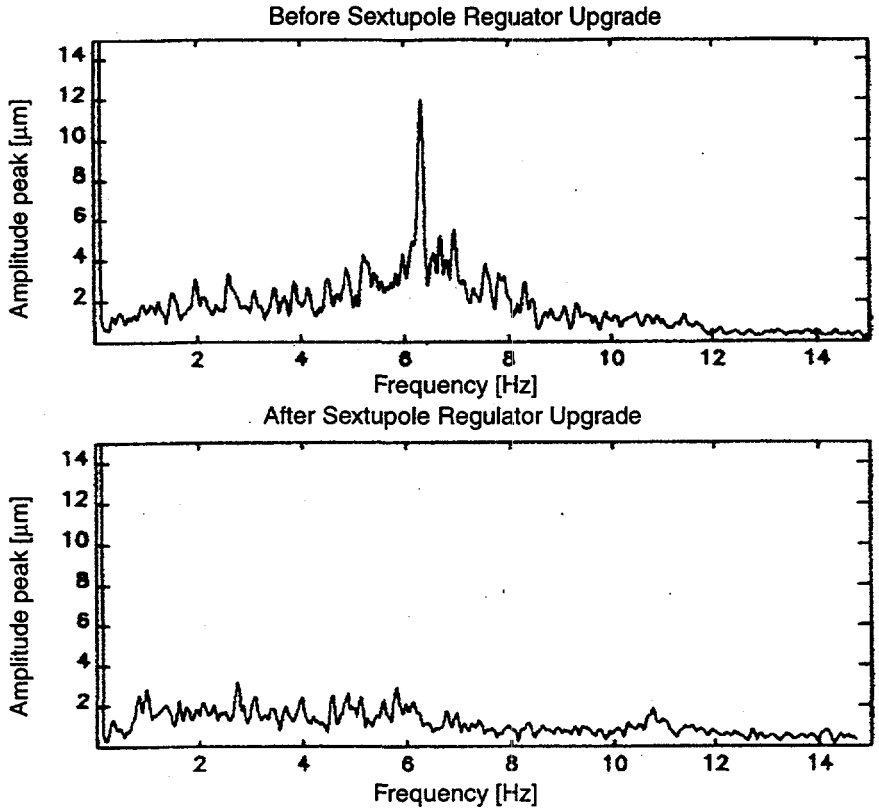

FIGURE 5. Observations of horizontal beam motion data before (upper) and after (lower) the sextupole power supply upgrade.

TABLE 2. Summary of Beam Motion Contributions Before and After the Sextupole Power Supply Corrective Step

Bandwidth	μm rms	Condition
1 → 15	26.9	Before
	15.5	After
5 → 8	21.9	Before
	8.5	After
9 → 12	5.9	Before
	5.3	After

Transverse Size

As reported previously (8), the first qualitative transverse measurements were in the single-turn, single-bunch beams of early operations. As the number of turns increased, the neutral density filters in front of the imaging camera were adjusted. The first stored beam at APS was actually done at ~ 4.2 GeV rather than 7 GeV due to rf power limitations in the first few months of 1995. By the summer of 1995 routine single-bunch studies were underway. Initial data from both the S35 OSR station and the sector-1 x-ray pinhole station were consistent with the 8.2-nm rad natural emittance, about 0.1% energy spread, and a vertical coupling noticeably lower than the 10% baseline design. As shown in Fig. 6, the horizontal size of σ_{xT} ~ 145 ± 25 μm includes contributions from the betatron emittance, the approximate 80 to 100 μm per 0.1% energy spread at this dispersive point in the lattice, and the limiting resolution terms. Equation 2 represents this:

$$\sigma_{xT} = [\beta_x \varepsilon + (\eta_x \sigma_\varepsilon)^2 + (\sigma_{res})^2]^{1/2} . \tag{2}$$

For these data the vertical size of $\sigma_{yT} = 84 \pm 20$ μm has a significant contribution from the $\sigma_{res} = 65 \pm 10$ μm term which is evaluated with a 550 × 40 nm bandpass filter. The deconvolved vertical size is $\sigma_y \approx 50$ μm which implies a vertical coupling of about 3%. At the baseline 10% coupling, a vertical size of 117 μm would be expected, and at 1% coupling a $\sigma_y = 39$ μm would be expected. These are beam size projections only, and the β functions are assumed to be within 10% of their design values. Subsequent tests included a parallel tracking of observed beam size with coupling, with the vertical size ranging from 50 to 120 μm. Measurements have also been performed as a function of single-bunch current and no significant size increase was observed from 0.2 to 7.7 mA. These measurements were all done with OSR imaging using a water-cooled Moly pick-off mirror whose properties were adequate up to 10 to 20 mA. The higher current runs will be addressed in a later section.

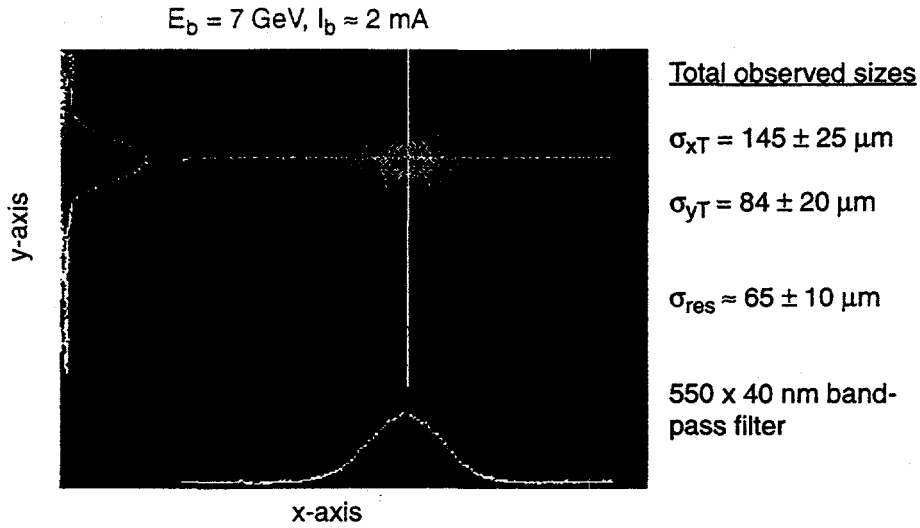

FIGURE 6. Transverse beam size measurements from OSR images. By removing the system resolution turn contribution, the horizontal size and vertical size are consistent with baseline values.

Bunch Length

The early bunch length and longitudinal profile measurements were done initially in single-bunch mode. Initial data shown in Fig. 7 at 3-mA stored beam current are from a run on July 27, 1995. Here the dual-sweep streak camera covers about 1000 ps on the fast axis and 10 μs on the slow axis. Three successive turns in the SR are displayed with 3.68-μs spacing. The nominal bunch length is ~ 102 ps (FWHM) or 43 ps (σ). With this transverse image being rotated in the transport optics to the streak camera, the horizontal axis actually displays the y profile of the beam distribution during a single micropulse. The longitudinal profile is near Gaussian although the data appear to fall at a slightly faster rate from the peak on the later-time side.

Such measurements were performed versus single-bunch beam current during experiments in August and October 1995. Figure 8 shows a plot of bunch length in ps versus current on the horizontal axis. The extensive elongation of the bunch (tripling) from 0.2 mA to 7.7 mA is noted. Analysis of this dependency based on the Chao-Gareyte parameter led to an estimate of the ring impedance of about 0.5 Ω (10). The estimated rf gap voltage was about 6.5 MV compared to the design goal of 9.5 MV.

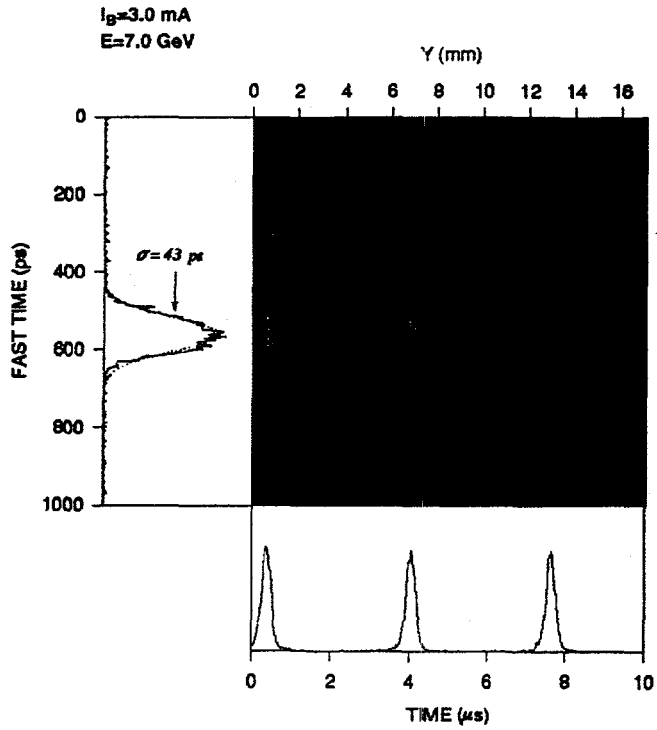

FIGURE 7. Dual-sweep streak camera images of single-bunch beam on three successive turns. The vertical axis is the fast time axis, and the horizontal axis has both 10-μs span and y-profile information.

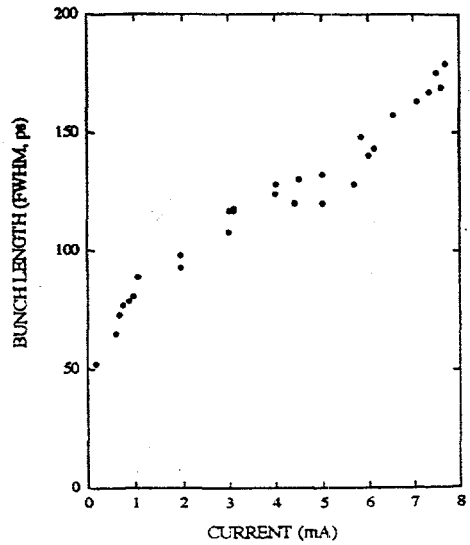

FIGURE 8. Plot of bunch length versus single-bunch current. Significant bunch lengthening with increased current was observed.

These effects are explored further in Fig. 9 where both the horizontal beam size and rms bunch length were tracked together in October 15, 1995 tests. Notable features include the relatively constant horizontal size of the beam in the dipole source point where the dispersion and energy spread product would produce the approximate horizontal sizes of 117, 147, and 215 μm for 0%, 0.1%, and 0.2% energy spread, respectively (see the dashed lines in the figure). The bunch again lengthens by almost a factor of two in comparison to the energy spread's feature. The low-current bunch length of 35 ps is consistent with even a lower rf gap voltage than the 6.5 MV in the August 19, 1995 run. Early assessments of these results indicate that the potential-well-distortion (PWD) model is more appropriate than the microwave instability model which would predict an energy spread larger than 0.2% at 7 mA stored beam current (10).

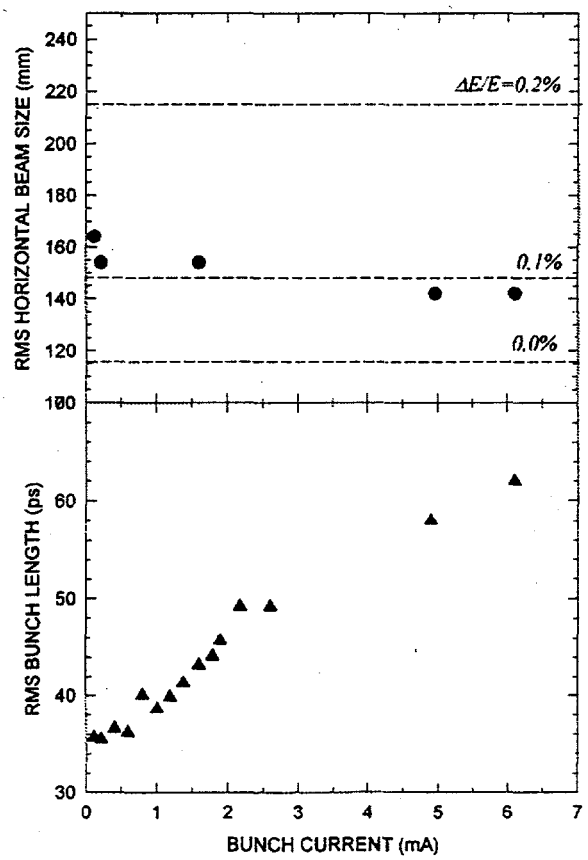

FIGURE 9. Measurements of rms horizontal beam size and rms bunch length versus single-bunch currents.

Vertical, Head-Tail Instability Observations

In an attempt to explore both measurement capability of the dual-sweep streak camera and the stable parameter space of the ring, the vertical, head-tail instability was purposely induced by decreasing the normal settings of the sextupole fields controlling vertical chromaticity. Although we initially injected and stored beam with all sextupoles off, they were needed for stored beam currents in a single bunch in excess of 1 mA to avoid the head-tail instability. The experiment was performed by first observing a dramatic increase in the transverse y-profile size in a standard OSR CCD-camera/image at about 3-mA stored beam current and decreased sextupole fields. Then the signature of the head-tail instability in a single micropulse was assessed with the dual-sweep streak camera. Figure 10(a) shows the streak images under stable conditions, and Fig. 10(b) shows the clear blurring of the y shape and the tilt in y-t space of the beam. Additionally the precession of the head-tail angle is tracked turn-by-turn in the 10-μs span or the 20-μs span. Figure 11 shows the y-t angle precesses one cycle in about four turns, and this may be connected with the fractional vertical betatron tune of 1/4. It is estimated that this instability will be controlled up to 10 to 15 mA in a single bunch with the installed sextupoles and power supplies.

HIGH CURRENT COMMISSIONING PHASE

The next thrust was to go for the baseline (100 mA) high stored beam currents. The practical aspect of machine protection against the high-powered x-ray beams from the dipole bending magnets and particularly the 10-kW insertion device (ID) beams immediately came to the forefront (11). In this section some aspects of the APS machine protection system (MPS) will be discussed as well as beam lifetime vs. vacuum chamber height, qualification of the DCCT, upgrades to the OSR photon monitor station, and actual ID closed-gap operations.

The APS storage ring is designed to be passively safe up to 100 mA from the bending magnet x-ray sources when all absorbers are properly in place and the water flow to the chambers and absorbers is as prescribed. In Fig. 12 a block diagram illustrates the architecture of the MPS which includes all the sensor inputs, the local MPS modules, the 1-MHz optical heartbeat, the main MPS module, and the rf abort features with an interruption of the low-level rf for 100 ms as the first action. The beam should coast in to the scraper in about 300 μs. Beam missteering in an ID straight is particularly threatening since the worst-case scenario allows about a 3-ms dwell time before the vacuum chamber integrity would be compromised.

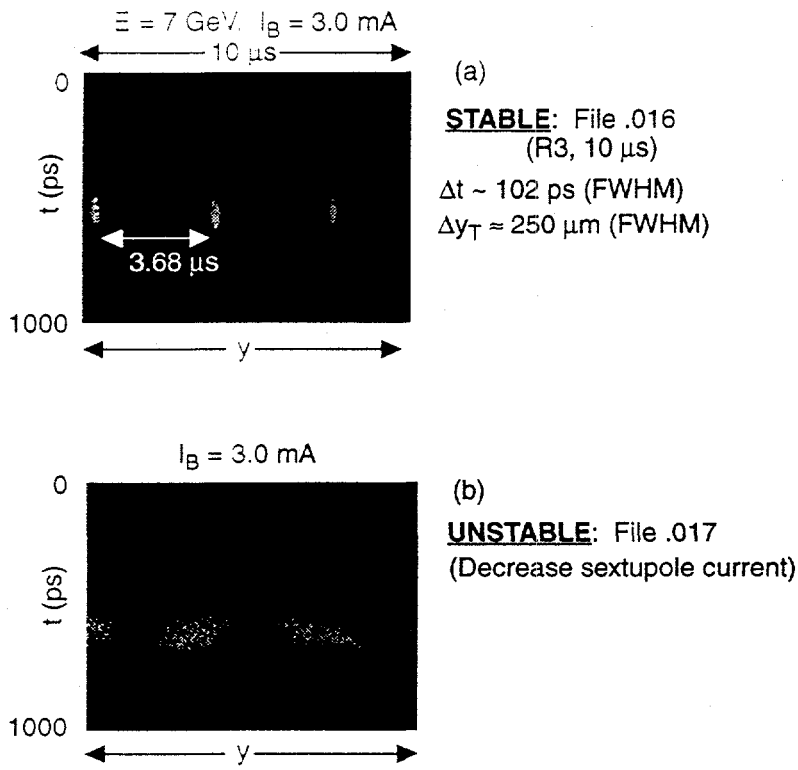

FIGURE 10. Dual-sweep streak images of the beam (a) without and (b) with the vertical, head-tail instability.

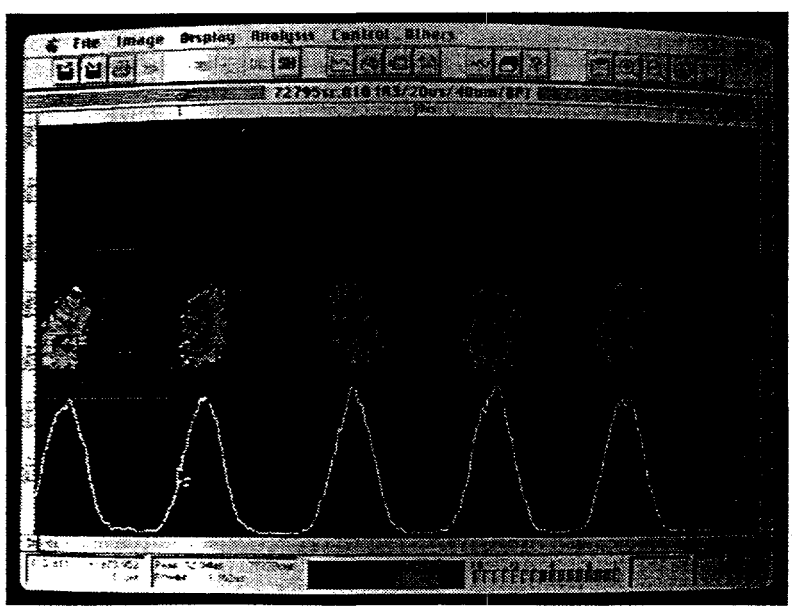

FIGURE 11. Dual-sweep streak image showing the precession of the y-t angle in about four turns.

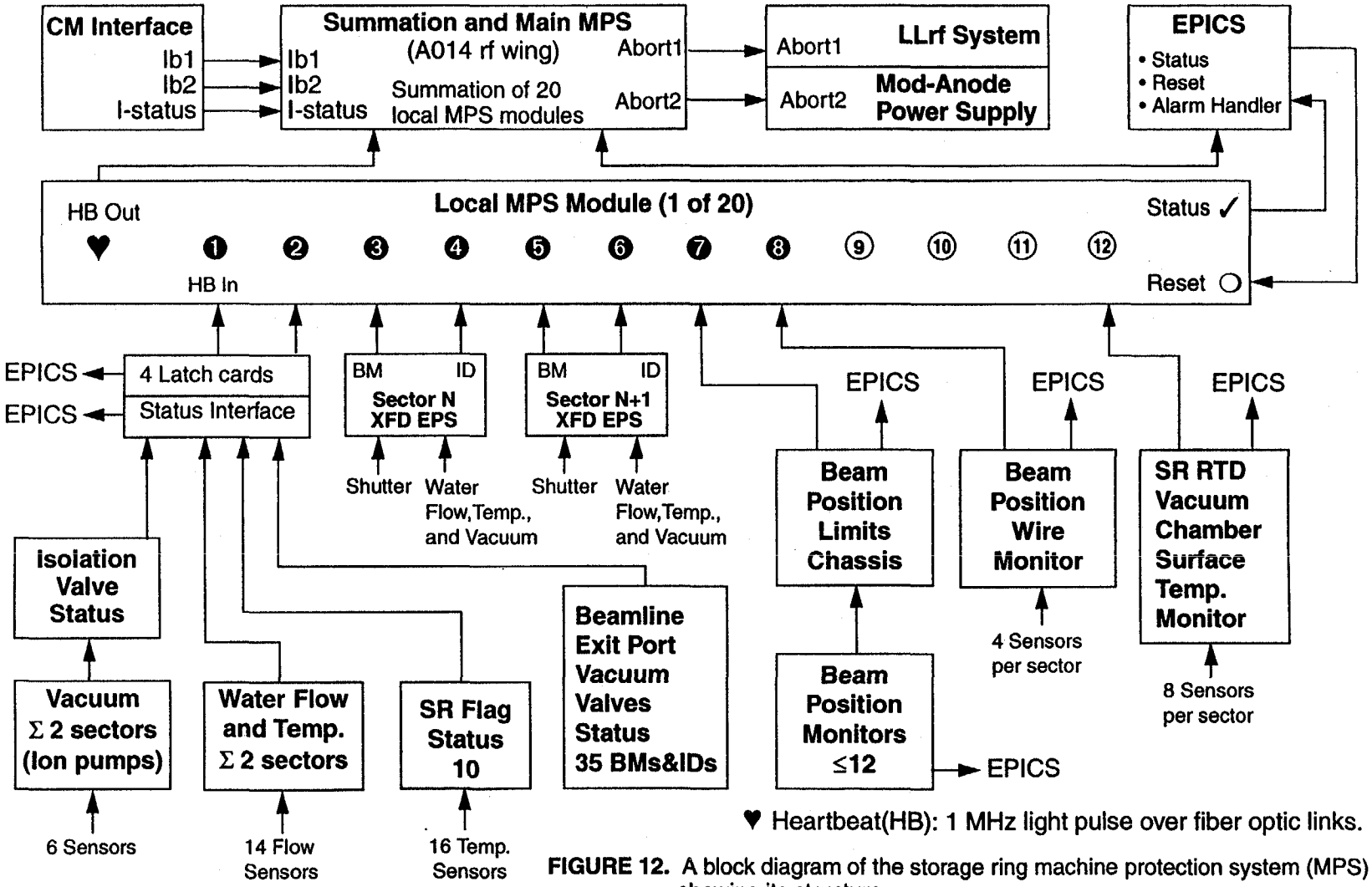

FIGURE 12. A block diagram of the storage ring machine protection system (MPS) showing its structure.

The beam position limits detector (BPLD) compares the rf BPM position readings to the preset limit of approximately ± 1.5 mm horizontally and ± 1 mm vertically. The first ID was operated with closed gap and at 100-mA stored beam current on January 26, 1996. At the time of this Workshop about six IDs and BPLDs had been commissioned. The phase I plan is 20 user IDs and one ID for particle beam characterizations.

One critical aspect of the BPLDs was the validation of the actual rf BPM offsets. These were determined by a beam-based technique using the variations of the nearby quadrupole strength and steering through the quad to determine the effective offset. Data are collected from 80 BPM locations in the ring. For the insertion device straight mini-BPMs, the standard rf BPM locations BP2 and AP2 on either side of the ID are evaluated, and a line is established to deduce the offsets for the mini-BPMs. Recent results are given in Table 3. The sector 1 ID is bounded by sector 1 and sector 2 rf BPMs. Offsets generally are in the 100- to 200-μm regime which are small compared to the trip limits at 1 to 1.5 mm. Cross-comparisons to x-BPMs in front ends were also done.

TABLE 3. Recent Results for Total Offsets of rf BPMs

ID#	BPM Location	X (mm)	Y (mm)
1	1BP1	0.132	–0.026
	2AP1	–0.267	–0.109
2	2BP1	0.046	0.137
	3AP1	0.020	–0.179
19*	19BP1	–0.657	0.134
	20AP1	0.186	–0.043

* S19 ID vacuum chamber warp?

As part of the evaluation of expected lifetime effects for the smaller gap chambers of 12-mm and 8-mm full gap, the vertical scrapers in the SR were used to simulate these apertures. Figure 13 shows the plot of the lifetime versus the half aperture. Lifetimes greater than five hours at low currents were achieved with the effective 8-mm full aperture. There was no measurable difference from the baseline 12-mm full aperture, so the project decided to proceed with the smaller-aperture chambers. This allows ID gaps down to about 10.5 mm and a much smoother coverage of x-ray energies from 5 to 70 keV. Lifetimes greater than five hours at low currents were achieved with the effective 8-mm full aperture.

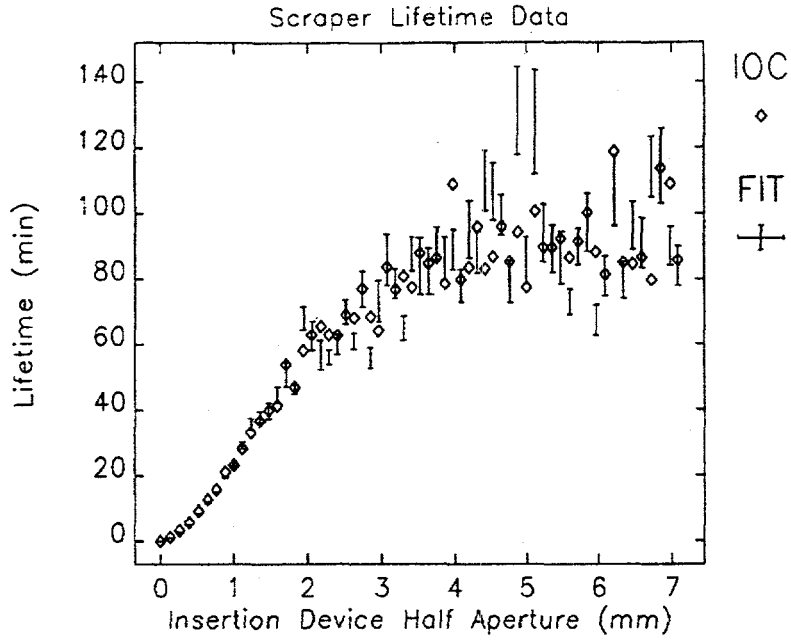

FIGURE 13. A plot of stored beam lifetime versus the half aperture. These data supported operations with the 8-mm full-aperture chamber.

Another commissioning point involved the measurement of the effects of the ID field error on the particle beam orbit. This is illustrated in Fig. 14 where the vertical orbit change around the circumference of the ring is observed between the open (45 mm) and closed (12.5 mm) gap condition. The data were measured and fit by M. Borland using the rf BPM system to detect the variation of orbit effects (1 to 10 μm) with the lattice positions and the vertical tune of about 14.3 (12).

Beam size measurements were taken with the x-ray pinhole camera at 70 to 100 mA. Transverse sizes of σ_x = 158 μm and σ_y ~ 117 μm now include the system resolution limit of about 80 μm in this first configuration as described elsewhere (9). The commissioning phase culminated with the successful storing of 100 mA in the ring as shown in the DCCT data of Fig. 15. The stored beam is electrons so the negative current is indicated in the figure around 22.6 and 23.1 to 23.4 hr on January 12, 1996. By May 1996 the baseline 10-hr lifetime at this current level also had been attained.

NEXT PHASE

Our next phase will include addressing the beam orbit stability with the use of a state-of-the-art digital feedback system. This system has been described previously (13), and its principles have been tested on other rings. Global tests were

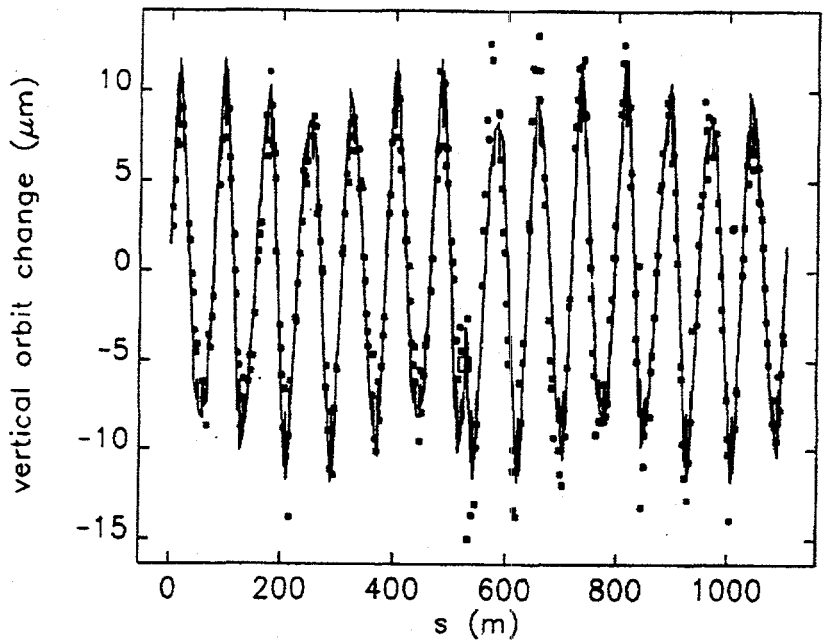

FIGURE 14. Comparison of measurement and simulation of the effects of the small ID field errors on the orbit.

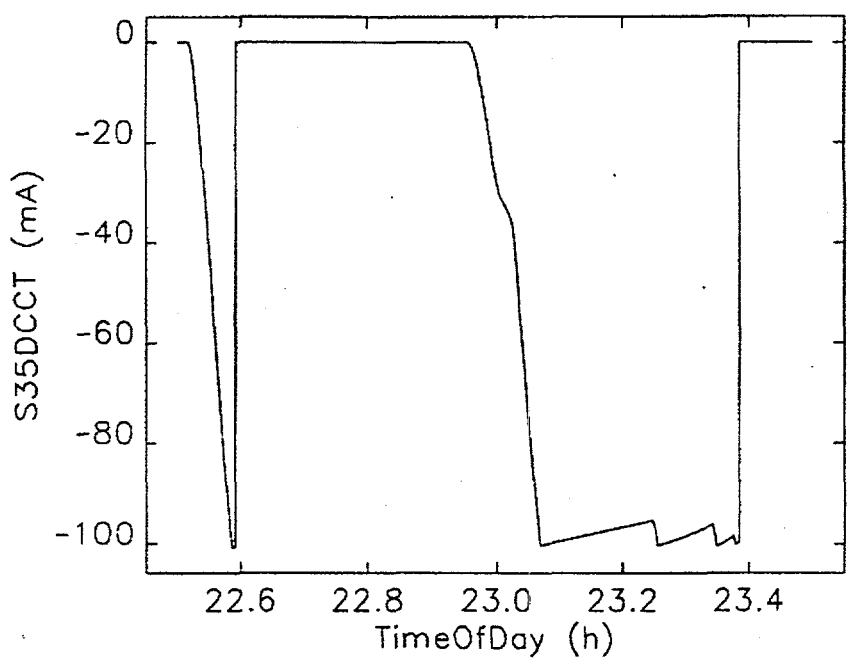

FIGURE 15. Plot of stored beam current versus time on the evening of January 12, 1996. First operations at 100-mA, the baseline objectives, are shown.

performed at SSRL, NSLS, and ESRF. A local feedback test was performed at ESRF. The hardware configuration is shown in Fig. 16 with additional discussion in another paper in these proceedings (14). The key features of on-board digital signal processors and the use of a reflective memory network to provide rf BPM information and corrector magnet power supply settings to each of 20 locations around the ring are important aspects of the system. As stated earlier, the orbit stability is near specifications for the baseline operations, but lower vertical coupling plans carry with them the need to stabilize the orbit even more in the future. The global feedback system is expected to be in commissioning in the Fall of 1996. A simulation of the global feedback system regime is given in Fig. 17. The closed-loop noise rejection is –20 dB at 10 Hz.

SUMMARY

In summary, both the machine and the installed SR diagnostics systems have now been commissioned for high current (80 to 100 mA) runs. The rf BPMs have demonstrated the required resolution and are now being evaluated for offset effects with bunch current or bunch pattern and long-term drift. The MPS system is operational, the phase 1 x-ray pinhole imaging station is installed, and enhanced measurement capabilities with a diagnostics undulator are in the future. The investigations of bunch length with stored beam current and head-tail instabilities have already been successfully initiated. It is expected that with additional rf power installed, operations at greater than 100 mA will follow.

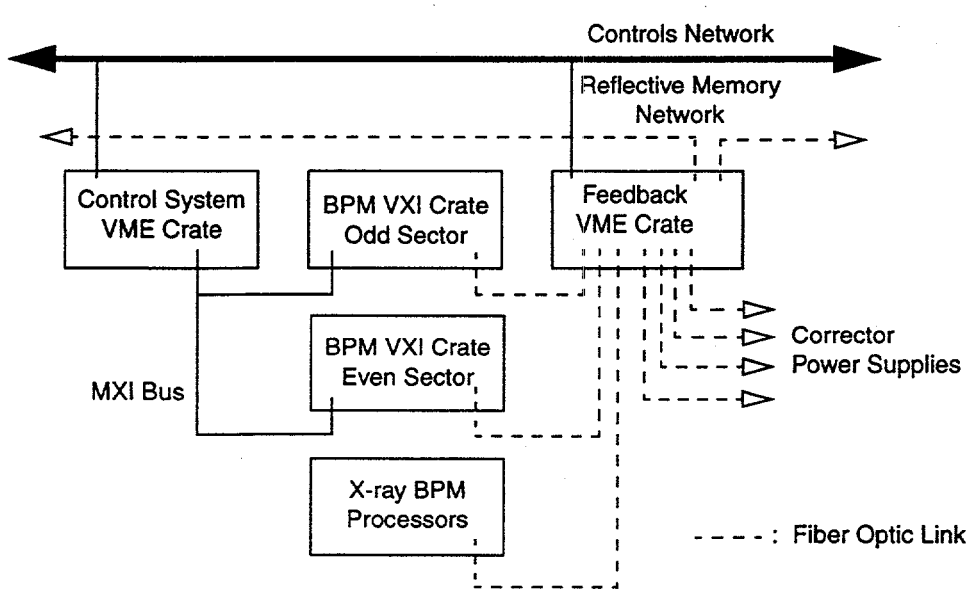

FIGURE 16. Hardware configuration of an orbit feedback station.

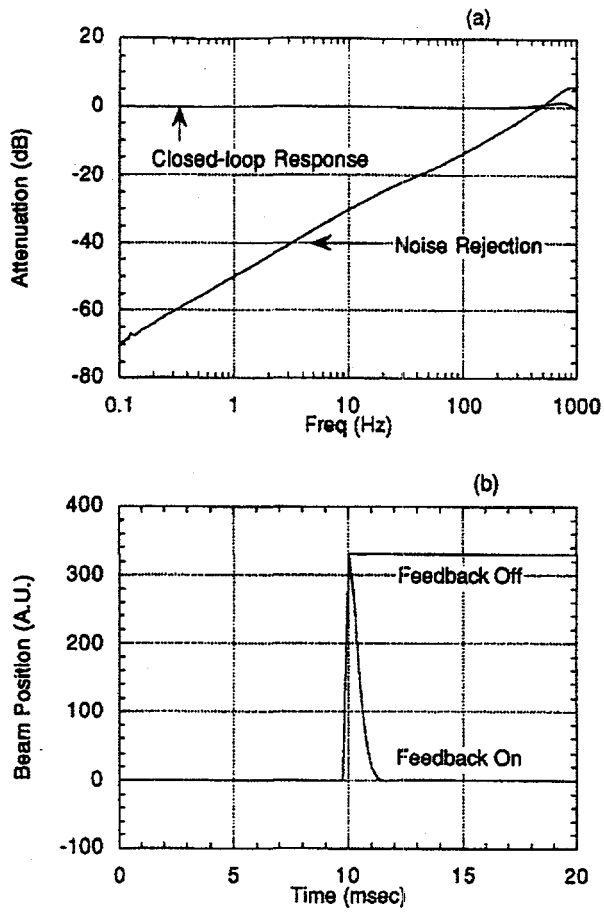

FIGURE 17. A simulation of the global feedback response to a step function displacement: (a) the attenuation vs. frequency and (b) the 1-ms response time.

ACKNOWLEDGMENTS

The author acknowledges the contributions of the ASD Diagnostics staff and technicians, the many hours of overlap with Mike Borland, Louis Emery, Glenn Decker, Steve Milton, and Nick Sereno in the main control room, and the support of John Galayda of the Accelerator Systems Division.

REFERENCES

1. Galayda, J. N., "The Advanced Photon Source," Proceedings of the 1995 Particle Accelerator Conference and International Conference on High-Energy Accelerators, Dallas, TX, May 1-5, 1995, 4-8, (1996).
2. Lumpkin, A. H. et. al., "Overview of Charged-Particle Beam Diagnostics for the Advanced Photon Source (APS)," Proceedings of the Fourth Accelerator Instrumentation Workshop, Berkeley, CA, Oct. 27-30, 1992, *AIP Conference Proceedings* **281**, 150-157 (1993).
3. Lumpkin, A. H. et al., "Initial Diagnostics Commissioning Results for the Advanced Photon Source (APS)," Proceedings of the 1995 Particle Accelerator Conference, Dallas, TX, May 1-5, 1995, 2473-2475 (1996) and references therein.
4. Kim, S. et al., "Investigation of Low-Frequency Beam Motion at the Advanced Photon Source," Proceedings of the Conference on Synchrotron Radiation Insrumentation, Oct. 17-20, 1995, *Rev. Sci. Instrum.* **67** (9), September 1996.
5. Kahana, E. and Chung, Y., "Commissioning Results of the APS Storage Ring RF Beam Position Monitors," these proceedings.
6. Wang, X, Lenkszus, F., and Rotela, E., "The Development of Beam Current Monitors in the APS," Proceedings of the 1995 Particle Accelerator Conference, Dallas, TX, May 1-5, 1995, 2464-2467 (1996).
7. Patterson, D., "Initial Commissioning Results from the APS Loss Monitor System," these proceedings.
8. Lumpkin, A. and Yang, B., "Status of the Synchrotron Radiation Monitors for the APS Facility Rings," Proceedings of the 1995 Particle Accelerator Conference, Dallas, TX, May 1-5, 1995, 2470-2472 (1996).
9. Yang, B. and Lumpkin, A., "Particle-Beam Profiling Techniques on the APS Storage Ring," these proceedings.
10. Chae, Y., (Argonne National Laboratory) private communication, October 1995.
11. Fuja, R. et. al. "The APS Machine Protection System (MPS)," these proceedings.
12. Borland, M., (Argonne National Laboratory) private communication, April 1996.
13. Chung, Y., "Beam Position Feedback System for the Advanced Photon Source," Proceedings of the 1993 Beam Instrumentation Workshop, *AIP Conference Proceedings* **319**, 1-20 (1994).
14. Barr, D. and Chung Y., "Hardware Design and Implementation of the Closed-Orbit Feedback System at APS," these proceedings.

DISCLAIMER

This report was prepared as an account of work sponsored by an agency of the United States Government. Neither the United States Government nor any agency thereof, nor any of their employees, makes any warranty, express or implied, or assumes any legal liability or responsibility for the accuracy, completeness, or usefulness of any information, apparatus, product, or process disclosed, or represents that its use would not infringe privately owned rights. Reference herein to any specific commercial product, process, or service by trade name, trademark, manufacturer, or otherwise does not necessarily constitute or imply its endorsement, recommendation, or favoring by the United States Government or any agency thereof. The views and opinions of authors expressed herein do not necessarily state or reflect those of the United States Government or any agency thereof.